

Coexistence of intrinsic piezoelectricity and ferromagnetism induced by small biaxial strain in septuple-atomic-layer VSi_2P_4

San-Dong Guo¹, Wen-Qi Mu¹, Yu-Tong Zhu¹ and Xing-Qiu Chen^{2,3}

¹*School of Electronic Engineering, Xi'an University of Posts and Telecommunications, Xi'an 710121, China*

²*Shenyang National Laboratory for Materials Science, Institute of Metal Research, Chinese Academy of Science, 110016 Shenyang, Liaoning, P. R. China and*

³*School of Materials Science and Engineering, University of Science and Technology of China, Shenyang 110016, P. R. China*

The septuple-atomic-layer VSi_2P_4 with the same structure of experimentally synthesized MoSi_2N_4 is predicted to be a spin-gapless semiconductor (SGS). In this work, the biaxial strain is applied to tune electronic properties of VSi_2P_4 , and it spans a wide range of properties upon the increasing strain from ferromagnetic metal (FMM) to SGS to ferromagnetic semiconductor (FMS) to SGS to ferromagnetic half-metal (FMHM). Due to broken inversion symmetry, the coexistence of ferromagnetism and piezoelectricity can be achieved in FMS VSi_2P_4 with strain range of 0% to 4%. The calculated piezoelectric strain coefficients d_{11} for 1%, 2% and 3% strains are 4.61 pm/V, 4.94 pm/V and 5.27 pm/V, respectively, which are greater than or close to a typical value of 5 pm/V for bulk piezoelectric materials. Finally, similar to VSi_2P_4 , the coexistence of piezoelectricity and ferromagnetism can be realized by strain in the VSi_2N_4 monolayer. Our works show that VSi_2P_4 in FMS phase with intrinsic piezoelectric properties can have potential applications in spin electronic devices.

PACS numbers: 71.20.-b, 77.65.-j, 72.15.Jf, 78.67.-n

Email:sandongyuwang@163.com

Keywords: Ferromagnetism, Piezoelectronics, 2D materials

I. INTRODUCTION

Due to the advantages of high speed, high integration density and high power transformers, the two-dimensional (2D) magnetic materials have great potential applications for nanoscale spintronic devices¹⁻³. A few types of 2D magnetic materials have been studied both in theory and in experiment⁴⁻⁹. For example, the $\text{Cr}_2\text{Ge}_2\text{Te}_6$ is an intrinsic ferromagnetic 2D material⁵, and the monolayer VS_2 and VSe_2 have also been experimentally demonstrated to be magnetic⁶. The $\text{Mn}_2\text{C}_6\text{S}_6\text{Se}_{12}$ and $\text{Mn}_2\text{C}_6\text{S}_6\text{Se}_6$ monolayers are predicted to be Dirac SGSs with 100% spin polarization, high Fermi velocities and high Curie temperatures⁷. Another particularly interesting property of 2D materials is piezoelectricity, which is used for energy conversion between electrical and mechanical energy. It has been theoretically reported that many kinds of 2D materials have significant piezoelectric coefficients¹⁰⁻¹⁶. Experimentally discovered piezoelectricity (such as MoS_2 ^{17,18}, MoSSe ¹⁹ and In_2Se_3 ²⁰) has promoted the huge studies on piezoelectric properties of 2D materials.

It is interesting and useful to combine the piezoelectricity and magnetism into the same kind of 2D material for applications in nanoscale spin electronic devices. The progress has been achieved in 2D vanadium dichalcogenides, and the VS_2 , VSe_2 and Janus- VSSe are not only magnetic semiconductors but also exhibit appreciable piezoelectricity²¹. Recently, the layered 2D MoSi_2N_4 and WSi_2N_4 have been synthesized by chemical vapor deposition (CVD)²². And then a new kind of 2D family MA_2Z_4 is proposed with α_i and β_i ($i=1$ to 6) phases by intercalating MoS_2 -type MZ_2 monolayer into InSe -type A_2Z_2 monolayer^{22,23}. Due to lacking inversion symmetry

of MA_2Z_4 with α_i phase, the piezoelectricity can exist, such as experimentally synthesized MoSi_2N_4 and WSi_2N_4 with α_1 phase²⁴. The α_1 - VSi_2P_4 is predicted to be a SGS²³, which may be easily tuned into FMS by strain. This will provide a platform to realize the coexistence of piezoelectricity and magnetism.

In this work, the biaxial strain effects on electronic properties of monolayer α_1 - VSi_2P_4 are studied by the first principle calculations. In considered strain range, the ferromagnetic (FM) ground state of VSi_2P_4 is confirmed, and it can change from FMM to SGS to FMS to SGS to FMHM with increasing strain. In FMS phase of VSi_2P_4 , the piezoelectricities are investigated, and the calculated d_{11} for 1%, 2% and 3% strains are 4.61 pm/V, 4.94 pm/V and 5.27 pm/V, respectively. Similar strain-induced phase transition can also be achieved in monolayer VSi_2N_4 , and only the critical point of phase transition is different from one of VSi_2P_4 . Our calculations show that the monolayer α_1 - VSi_2P_4 may be promising candidate for spintronic and piezoelectric applications by strain engineering.

The rest of the paper is organized as follows. In the next section, we shall give our computational details and methods. In the third section, we shall present main results of septuple-atomic-layer VSi_2P_4 . Finally, we shall give our discussion and conclusions in the fourth section.

II. COMPUTATIONAL DETAIL

Calculations are based on spin-polarized density functional theory (DFT)²⁵ using the popular generalized gradient approximation of Perdew, Burke and Ernzerhof (GGA-PBE)²⁶ as the exchange-correlation functional.

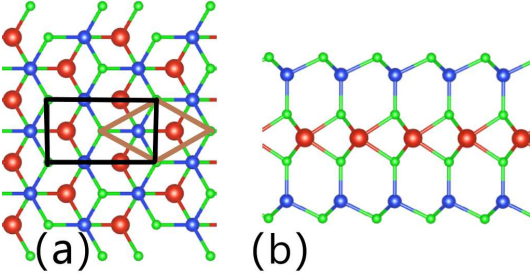


FIG. 1. (Color online) The (a) top view and (b) side view of crystal structure of monolayer VSi_2P_4 . The large red balls represent V atoms, and the middle blue balls for Si atoms, and the small green balls for P atoms. The primitive cell and rectangle supercell are marked by brown and black lines, respectively.

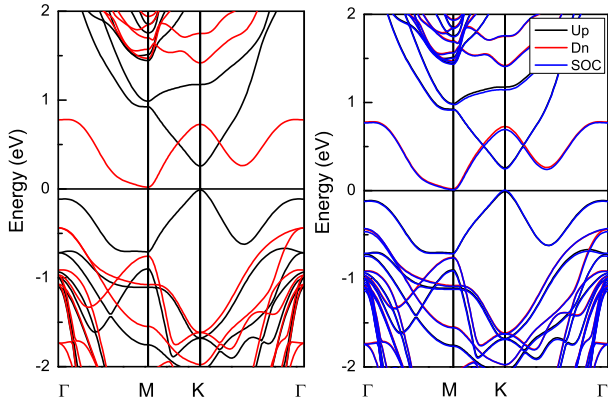


FIG. 2. (Color online) The energy band structures of unstrained VSi_2P_4 , include using GGA (Left) or GGA+SOC and GGA (Right) with FM state.

Projector augmented wave (PAW) potentials are used in all calculations, as implemented in the plane-wave code VASP^{27–29}. A vacuum spacing of more than 32 Å is used in the direction normal to the 2D monolayer in order to avoid interactions between two neighboring images. The kinetic energy cutoff is set to 500 eV, and the total energy convergence criterion is set to 10^{-8} eV. The ionic relaxation is performed until the force on each atom is less than $0.0001 \text{ eV} \cdot \text{Å}^{-1}$. Piezoelectricity is studied by using density functional perturbation theory (DFPT)³⁰. The reciprocal space is represented by the Monkhorst-Pack special k-point scheme with $15 \times 15 \times 1$ meshes for the calculations of electronic structure and elastic coefficients C_{ij} , and $9 \times 16 \times 1$ grid meshes for the energy of different magnetic configurations and piezoelectric stress coefficients e_{ij} . The 2D elastic coefficients C_{ij}^{2D} and piezoelectric stress coefficients e_{ij}^{2D} have been renormalized by $C_{ij}^{2D} = Lz C_{ij}^{3D}$ and $e_{ij}^{2D} = Lz e_{ij}^{3D}$, where the Lz is the length of unit cell along z direction.

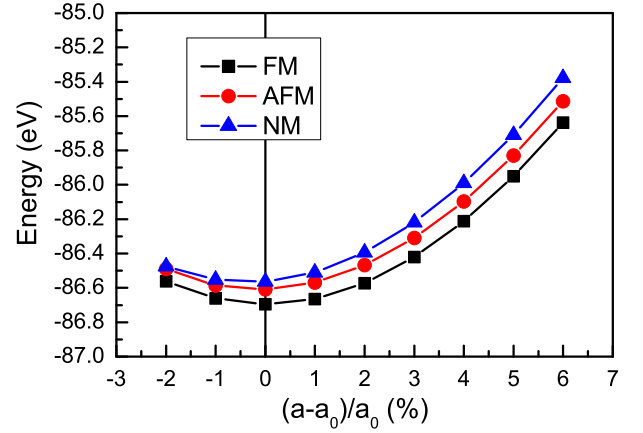


FIG. 3. (Color online) Calculated energy of FM state, AFM state and NM state as a function of strain with rectangle supercell.

III. MAIN CALCULATED RESULTS

The α_1 - VSi_2P_4 is predicted to be a parabolic FM SGS with the total magnetic moment $1.0 \mu_B$ ²³. Firstly, we relax the geometric structures of VSi_2P_4 with spin-polarized calculations, which is plotted in Figure 1. The seven atomic layers of N-Si-N-V-N-Si-N are observed with a VN_2 layer sandwiched between two Si-N bilayers. The optimized lattice constants is 3.486 Å, which is in good agreement with the previous theoretical result²³. We calculate electronic band structures of VSi_2P_4 using GGA and GGA plus spin orbital coupling (SOC), which are plotted in Figure 2. It is clearly seen that the Fermi energy level happens to touch the minority-spin conduction band minimum (CBM) at M point and the majority-spin valence band maximum (VBM) at K point at the same time, and a SGS is achieved. Calculated results show that the SOC has little effects on energy bands of VSi_2P_4 , so we use GGA to investigate the role of strain on the electronic structures of VSi_2P_4 .

Strain is a very effective way to tune the electronic structures, topological properties, transport and piezoelectric properties of 2D materials^{31–34}. The biaxial strain can be simulated by $(a - a_0)/a_0$ with a and a_0 being the strained and unstrained lattice constants. To determine the ground state of strained VSi_2P_4 , a rectangle supercell (in Figure 1) is used to construct two different initial magnetic configurations, including antiferromagnetic (AFM) and FM states. The energy of FM state, AFM state and non-magnetic (NM) state as a function of strain are shown in Figure 3. It is clearly seen that VSi_2P_4 prefers FM ground state in considered strain range, and the energy difference between AFM and FM states increases from 73 meV to 124 meV, when the strain changes from -2% to 6%. This means that the applied biaxial strain can effectively enhance the magnetic coupling of VSi_2P_4 , increasing the Curie temperature.

The energy band structures of FM VSi_2P_4 using GGA

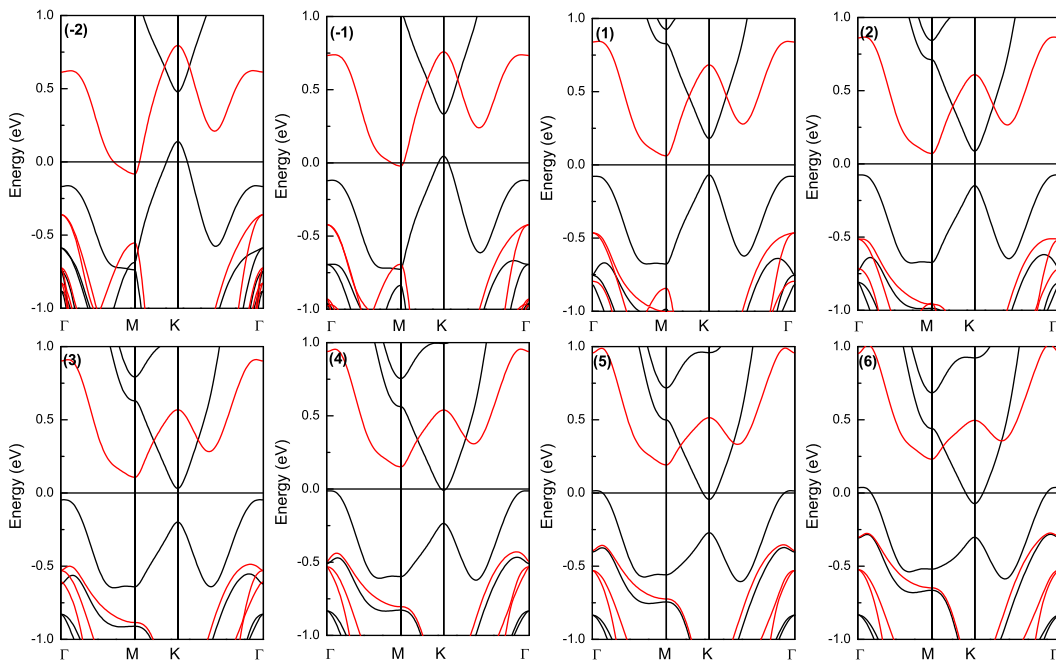


FIG. 4. (Color online) The energy band structures of FM VSi₂P₄ using GGA with strain from -2% to 6% except 0%, which has been shown in Figure 2. The black and red lines represent the spin-up and spin-down bands.

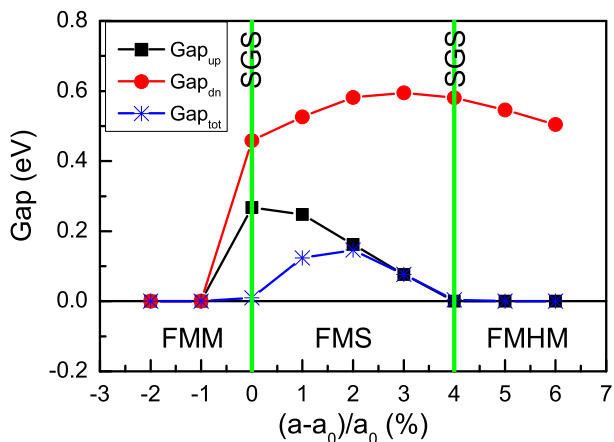


FIG. 5. (Color online) The majority-spin gap (Gap_{up}), the minority-spin gap (Gap_{dn}) and the total gap (Gap_{tot}) of FM VSi₂P₄ as a function of strain using GGA. The electronic properties change from FMM to SGS to FMS to SGS to FMHM with the increasing strain.

with strain from -2% to 6% except 0% are shown in Figure 4, and the majority-spin, minority-spin and total gaps are plotted in Figure 5. From -2% to 6%, the first conduction band of majority-spin moves toward the lower energy, and touches exactly the Fermi level at 4% strain, and then crosses the the Fermi level at >4% strain. The similar trend can be observed for the first conduction band of minority-spin, when the strain changes from 6% to -2%, and happen to touch the Fermi level at 0% strain. For the first valence band of majority-spin, the energy

eigenstates around the K point vary toward lower energy with strain from -2% to 6%, and touch the Fermi level at 0% strain, while the energy eigenstates around the Γ point move toward higher energy, and contact the Fermi level at 4% strain. These lead to diverse properties of VSi₂P₄ upon strain from FMM to SGS to FMS to SGS to FMHM. The compressive strain makes both majority-spin and minority-spin gaps be zero, and a FMM is achieved. When the tensile strain is less than 4%, both majority-spin and minority-spin gaps are nonzero, and then the total gap is positive value. In this strain range, a FMS can be induced by tensile strain. With tensile strain being larger than 4%, only minority-spin gap is nonzero, and the majority-spin gap become zero, which gives rise to a FMHM. At the critical states of 0% and 4%, the SGS can be observed, but they are different. At 0% strain, there is a gap for both the majority and minority channels, while there is no gap between the majority channel in the valence band and the minority channel in the conduction band. At 4% strain, the majority channel is gapless, while the minority channel is separated by a gap. Similar stress-tuned SGS can be observed in the ferromagnetic semiconductor HgCr₂Se₄³⁵.

The VSi₂P₄ has the $\bar{6}m2$ point group, and then lacks the inversion symmetry, which makes VSi₂P₄ to be piezoelectric. A piezoelectric material should be a semiconductor to prohibit current leakage. It is interesting to investigate the piezoelectric properties of VSi₂P₄ with the strain range of 0% to 4%, because the coexistence of piezoelectricity and magnetism can be achieved in the same kind of material. The piezoelectric stress tensors e_{ijk} and strain tensor d_{ijk} can be used to characterize the

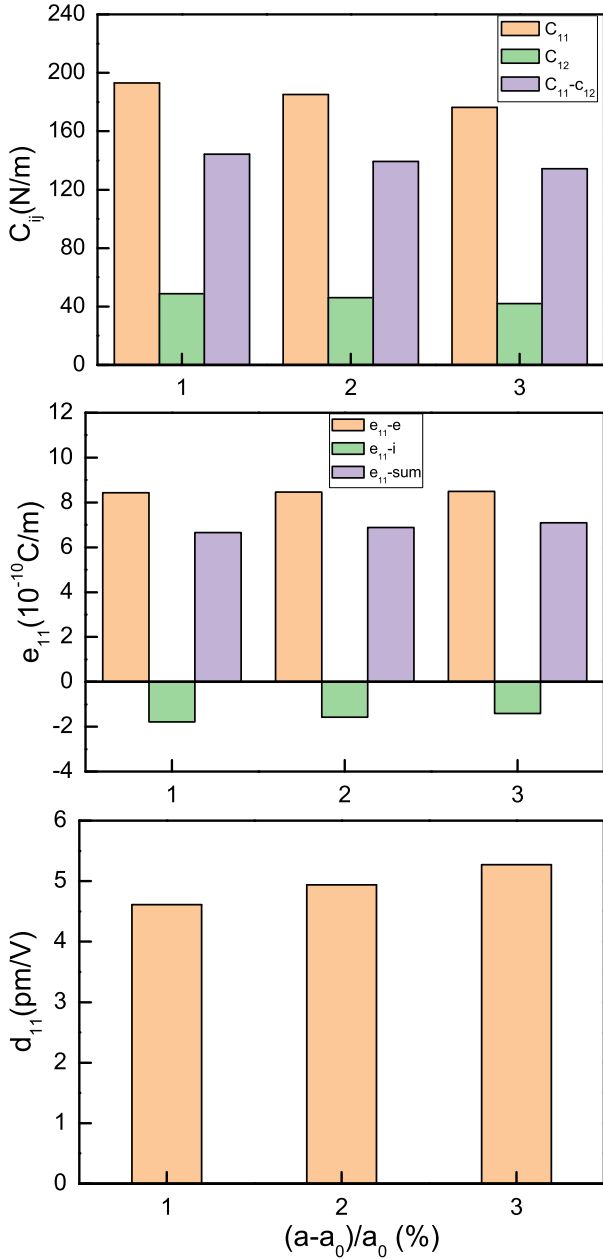


FIG. 6. (Color online) For monolayer VSi_2P_4 , (Top) the elastic constants C_{ij} , (Middle) piezoelectric stress coefficients e_{11} along with the ionic contribution and electronic contribution, and (Bottom) piezoelectric strain coefficients d_{11} with the strain being 1%, 2% and 3%.

linear piezoelectric effect of monolayer VSi_2P_4 , which include ionic and electronic contributions. Using the Voigt notation, the e_{ijk} and d_{ijk} can be represented as e_{ij} and d_{ij} , respectively. The e_{ik} is connected with d_{ij} by:

$$e_{ik} = d_{ij}C_{jk} \quad (1)$$

For 2D semiconductors, in general, in-plane stresses and strains are only allowed, while the out-of-plane is strain/stress free^{10,13,15}. For $\bar{6}m2$ point group, the C_{ij} ,

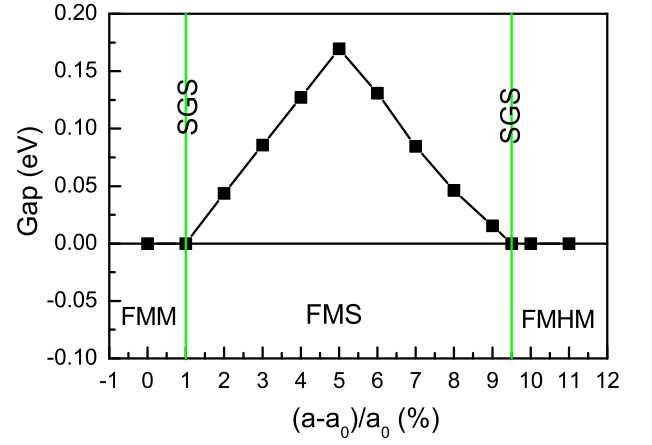


FIG. 7. (Color online) The total gap (Gap) of FM VSi_2N_4 as a function of strain using GGA. The electronic properties change from FMM to SGS to FMS to SGS to FMHM with the increasing strain.

e_{ij} and d_{ij} of monolayer VSi_2P_4 become:

$$\begin{pmatrix} e_{11} & -e_{11} & 0 \\ 0 & 0 & -e_{11} \\ 0 & 0 & 0 \end{pmatrix} \quad (2)$$

$$\begin{pmatrix} d_{11} & -d_{11} & 0 \\ 0 & 0 & -2d_{11} \\ 0 & 0 & 0 \end{pmatrix} \quad (3)$$

$$\begin{pmatrix} C_{11} & C_{12} & 0 \\ C_{12} & C_{11} & 0 \\ 0 & 0 & \frac{C_{11}-C_{12}}{2} \end{pmatrix} \quad (4)$$

Solving the about equations, the only independent in-plane d_{11} is:

$$d_{11} = \frac{e_{11}}{C_{11} - C_{12}} \quad (5)$$

A rectangle supercell is used for the calculation of e_{ij} , as shown in Figure 1. The C_{ij} are calculated by using strain-stress relationship. The elastic constants C_{ij} , piezoelectric stress coefficients e_{11} along with the ionic contribution and electronic contribution, and piezoelectric strain coefficients d_{11} of monolayer VSi_2P_4 with the strain being 1%, 2% and 3% are shown in Figure 6. All calculated elastic coefficients of VSi_2P_4 with the strain being 1%, 2% and 3% satisfy the Born stability criteria³⁶. It is found that the ionic and electronic parts have opposite contributions to e_{11} . The increasing strain can enhance the e_{11} , and these values for 1%, 2% and 3% strains are 6.65×10^{-10} C/m, 6.88×10^{-10} C/m and 7.09×10^{-10} C/m, respectively. The trend is mainly due to decreased ionic contribution (absolute value). The corresponding values of d_{11} for 1%, 2% and 3% strains are 4.61 pm/V,

4.94 pm/V and 5.27 pm/V, respectively. The strain-improved d_{11} is due to the enhanced e_{11} and reduced C_{11} - C_{12} according to Equation 5. These results are comparable with or larger than ones of TMD monolayers such as MoS₂ obtained from DFT calculations^{13,15}. The values of d_{11} of FMS VSi₂P₄ are greater than or close to a typical value for bulk piezoelectric materials, about 5 pm/V¹³. This indicates that FMS VSi₂P₄ caused by small strain show potential in piezoelectric devices.

The VSi₂N₄ has the same crystal structure with VSi₂P₄, and is predicted to be a FMM with the total magnetic moment 0.97 μ_B ²³, which is very close to 1.0 μ_B . This makes us believe that small strain may induce FMM to FMS transition. Firstly, the ground state of VSi₂N₄ is determined to be FM in the strain range of 0% to 11% by comparing the energy of FM, AFM and NM, and their energy bands are calculated. The total gap of FM VSi₂N₄ as a function of strain using GGA is plotted in Figure 7. It is found that only about 1% strain can make VSi₂N₄ become FMS, which can be maintained in the strain range of 1% to 9.5%. When the strain increases, the electronic properties of VSi₂N₄ vary from FMM to SGS to FMS to SGS to FMHM, which is the same with VSi₂P₄. The piezoelectric properties of VSi₂N₄ at 3% strain are studied as a representative. The calculated C_{11} and C_{12} are 431.17 N/m and 117.61 N/m, respectively, and the e_{11} is 6.71×10^{-10} C/m. According to Equation 5, the d_{11} can be attained for 2.14 pm/V.

IV. DISCUSSION AND CONCLUSION

It is well known that GGA underestimates semiconductor gap, and the hybrid functional HSE06 may give a more appropriate gap. However, for MoSi₂N₄ monolayer, the HSE06 overestimates its gap. The calculations

show that MoSi₂N₄ monolayer is an indirect gap semiconductor with the gap of 1.744 eV (GGA) or 2.297 eV (HSE06), and the experimental value is 1.94 eV²². It is found that the GGA gap is more closer to the experimental value than HSE06 one. So, it may be more suitable for VSi₂P₄ to use GGA to study its electronic properties. For VSi₂P₄ monolayer, the GGA may underestimate its gap, but our conclusion should be qualitatively correct, and only the critical points of phase transition change.

We have demonstrated that strain can effectively tune the electronic properties of VSi₂P₄ monolayer through first-principles simulations. The results show that FM state in considered strain range is more energetically preferred than AFM and NM states for VSi₂P₄ monolayer. With the increasing strain, the electronic properties of VSi₂P₄ vary from FMM to SGS to FMS to SGS to FMHM. The corresponding values of d_{11} of VSi₂P₄ in FMS phase for 1%, 2% and 3% strains are 4.61 pm/V, 4.94 pm/V and 5.27 pm/V, respectively, which are greater than 5 pm/V, a typical value for bulk piezoelectric materials. Similar strain dependence of electronic properties can also be achieved in monolayer VSi₂N₄, and the piezoelectricity and ferromagnetism can also coexist by strain tuning. The VSi₂P₄ and VSi₂N₄ may be promising 2D materials for applications in nanoscale spin electronic devices due to the combination of piezoelectric and magnetic properties.

ACKNOWLEDGMENTS

This work is supported by the Natural Science Foundation of Shaanxi Provincial Department of Education (19JK0809). We are grateful to the Advanced Analysis and Computation Center of China University of Mining and Technology (CUMT) for the award of CPU hours and WIEN2k/VASP software to accomplish this work.

-
- ¹ X. Lin, W. Yang, K. L. Wang, W. Zhao, Nat. Electron. **2**, 274 (2019).
² I. Choudhuri, P. Bhauriyal and B. Pathak, Chem. Mater. **31**, 8260 (2019).
³ Y. Sun, Z. Zhuo, X. Wu and J. Yang, Nano Lett. **17**, 2771 (2017).
⁴ Y. Ma, Y. Dai, M. Guo, C. Niu, Y. Zhu and B. Huang, ACS Nano, **6**, 1695 (2012).
⁵ C. Gong, L. Li, Z. Li, H. Ji, A. Stern, Y. Xia, T. Cao, W. Bao, C. Wang, Y. Wang, Z. Q. Qiu, R. J. Cava, S. G. Louie, J. Xia and X. Zhang, Nature **546**, 265 (2017).
⁶ Y. Guo, H. Deng, X. Sun, X. Li, J. Zhao, J. Wu, W. Chu, S. Zhang, H. Pan, X. Zheng, X. Wu, C. Jin, C. Wu and Y. Xie, Adv. Mater. **29**, 1700715 (2017).
⁷ X. M. Wu, Y. L. Feng, S. Li, B. Q. Zhang and G. Y. Gao, J. Phys. Chem. C **124**, 16127 (2020).
⁸ B. Huang, G. Clark, E. Navarro-Moratalla, D. R. Klein, R. Cheng, K. L. Seyler, D. Zhong, E. Schmidgall, M. A. McGuire, D. H. Cobden, W. Yao, D. Xiao, P. Jarillo-Herrero and X. Xu, Nature **546**, 270 (2017).
⁹ L. Dong, H. Kumar, B. Anasori, Y. Gogotsi and V. B. Shenoy, J. Phys. Chem. Lett. **8**, 422 (2017).
¹⁰ L. Dong, J. Lou and V. B. Shenoy, ACS Nano, **11**, 8242 (2017).
¹¹ Y. Xu, Z. Q. Li, C. Y. He, J. Li, T. Ouyang, C. X. Zhang, C. Tang and J. X. Zhong Appl. Phys. Lett. **116**, 023103 (2020).
¹² S. D. Guo, X. S. Guo, Z. Y. Liu and Y. N. Quan, J. Appl. Phys. **127**, 064302 (2020).
¹³ M. N. Blonsky, H. L. Zhuang, A. K. Singh and R. G. Hennig, ACS Nano, **9**, 9885 (2015).
¹⁴ R. X. Fei, W. B. Li, J. Li and L. Yang, Appl. Phys. Lett. **107**, 173104 (2015).
¹⁵ K. N. Duerloo, M. T. Ong and E. J. Reed, J. Phys. Chem. Lett. **3**, 2871 (2012).
¹⁶ Y. Chen, J. Y. Liu, J. B. Yu, Y. G. Guo and Q. Sun, Phys. Chem. Chem. Phys. **21**, 1207 (2019).
¹⁷ W. Wu, L. Wang, Y. Li, F. Zhang, L. Lin, S. Niu, D.

- Chenet, X. Zhang, Y. Hao, T. F. Heinz, J. Hone and Z. L. Wang, *Nature* **514**, 470 (2014).
- ¹⁸ H. Zhu, Y. Wang, J. Xiao, M. Liu, S. Xiong, Z. J. Wong, Z. Ye, Y. Ye, X. Yin and X. Zhang, *Nat. Nanotechnol.* **10**, 151 (2015).
- ¹⁹ A. Y. Lu, H. Zhu, J. Xiao, C. P. Chuu, Y. Han, M. H. Chiu, C. C. Cheng, C. W. Yang, K. H. Wei, Y. Yang, Y. Wang, D. Sokaras, D. Nordlund, P. Yang, D. A. Muller, M. Y. Chou, X. Zhang and L. J. Li, *Nat. Nanotechnol.* **12**, 744 (2017).
- ²⁰ M. Dai, Z. Wang, F. Wang, Y. Qiu, J. Zhang, C. Y. Xu, T. Zhai, W. Cao, Y. Fu, D. Jia, Y. Zhou, and P. A. Hu, *Nano Lett.* **19**, 5416 (2019).
- ²¹ J. H. Yang, A. P. Wang, S. Z. Zhang, J. Liu, Z. C. Zhong and L. Chen, *Phys. Chem. Chem. Phys.*, **21**, 132 (2019).
- ²² Y. L. Hong, Z. B. Liu, L. Wang et al., *Science* **369**, 670 (2020).
- ²³ L. Wang, Y. P. Shi, M. F. Liu et al., arXiv:2008.02981 (2020).
- ²⁴ S. D. Guo, Y. T. Zhu and W. Q. Mu, arXiv:2008.05751 (2020).
- ²⁵ P. Hohenberg and W. Kohn, *Phys. Rev.* **136**, B864 (1964);
- W. Kohn and L. J. Sham, *Phys. Rev.* **140**, A1133 (1965).
- ²⁶ J. P. Perdew, K. Burke and M. Ernzerhof, *Phys. Rev. Lett.* **77**, 3865 (1996).
- ²⁷ G. Kresse, *J. Non-Cryst. Solids* **193**, 222 (1995).
- ²⁸ G. Kresse and J. Furthmüller, *Comput. Mater. Sci.* **6**, **15** (1996).
- ²⁹ G. Kresse and D. Joubert, *Phys. Rev. B* **59**, 1758 (1999).
- ³⁰ X. Wu, D. Vanderbilt and D. R. Hamann, *Phys. Rev. B* **72**, 035105 (2005).
- ³¹ E. Scalise, M. Houssa, G. Pourtois, V. Afanas'ev and A. Stesmans, *Nano Res.* **5**, 43 (2012).
- ³² H. K. Liu, G. Z. Qin, Y. Lin and M. Hu, *Nano Lett.* **16**, 3831 (2016).
- ³³ N. Jena, Dimple, S. D. Behere and A. D. Sarkar, *J. Phys. Chem. C* **121**, 9181 (2017).
- ³⁴ Dimple, N. Jena, A. Rawat, R. Ahammed, M. K. Mohanta and A. D. Sarkar, *J. Mater. Chem. A* **6**, 24885 (2018).
- ³⁵ S. D. Guo and B. G. Liu, *J. Phys.: Condens. Matter* **24**, 045502 (2012).
- ³⁶ R. C. Andrew, R. E. Mapasha, A. M. Ukpong and N. Chetty, *Phys. Rev. B* **85**, 125428 (2012).